



CT imaging of Lindner tested, burnt timber

András Biró¹ · Éva Lublós¹

Received: 16 May 2023 / Accepted: 7 November 2023 / Published online: 2 December 2023
© The Author(s) 2023

Abstract

The durability of fire-retardant materials used for wooden structures and wood-based products can be evaluated on small cut-out samples with the so-called Lindner test, which is a standard procedure in Hungary where 1 g of hexamethylene-tetramine is burnt under the wooden specimen and the mass loss is measured. For further spatial information about the burnt part of the samples, the specimens were CT scanned after the Lindner test. The goal was to evaluate if the charred part can be properly segmented in a CT image set and if the two measurements combined are precise enough to provide charring rate data. With the segmentation of the CT image sets, the burnt volumes could be separated properly in each case even when knots were present. Spruce sample provided the most consistent results regarding the mass loss/burnt volume. This is probably due to the uneven ring spacing and other inhomogeneities in the density of oak and ash.

Keywords Timber · Charring-rate · CT · Lindner-test

Introduction

Timber is a combustible material so proper fire protection must be provided. This should be considered in the design phase of a construction when choosing materials. There are several recent publications regarding the fire performance of timber connections and timber products [1–7], which include both experimental and numerical analyses.

Regueira et al. [1] did two experimental fire tests to evaluate the fire performance of rounded dovetail connections as there are no design guidelines for this connection type in the European fire safety standard for timber construction (Eurocode 5-1-2) [8]. The authors also approached the problem from a numerical analysis point of view based on the general recommendations of the aforementioned standard. They concluded the following:

- The tested structural setup does not meet the R30 requirements, it maintained its load bearing capacity for 12 min.

- Original finite element (FE) model (FEM) based on the Eurocode 5 instructions showed lower temperatures in the connection than what was obtained from the experiments.
- A modified version of the model followed the experimental data better. In this case the heat transfer inside the connection was simulated via convection instead of conduction; therefore, these kinds of connections are not self-protected in fire.
- Thermal fluxes applied in the inner faces of the mortise cavity also led to simulation results to be in better agreement with the experiments.

Kleinhenz et al. [2] tested cross-laminated timber (CLT) rib panels in fire with the goal of improving and extending the design rules of the EN 1995-1-2 standard [8], because the fire behaviour and resistance of these are not yet covered by it. The reference mechanical tests for load bearing capacity as T sections at normal temperatures were in good agreement with the calculations from EN 1995-1-1 [9] using of effective width. Further tests also showed the importance of the glue line and a good quality screw-press gluing (SPG), because the adhesion layer can be the point of premature failure. The simplified calculation method from EN 1995-1-2 [8] gave a good estimate regarding charring depth of glulam (glued-laminated) ribs, but the overall fire performance was underestimated by

✉ András Biró
biro.andras@emk.bme.hu
Éva Lublós
lubloy.eva@emk.bme.hu

¹ Department of Construction Materials and Technologies,
Budapest University of Technology and Economics,
Műegyetem rkp 3, Budapest 1111, Hungary

the calculations because of the conservative estimation of the effective width in fire and the effect of the rounding corners.

Gernay [3] investigated the full burnout of timber columns and showed both experimentally and with simulation that these structures are susceptible to failure during the cooling phase in case of standardized natural fire curves with a cooling phase. This is due to the delayed heating and loss of mechanical properties at relatively low temperatures.

Wiesner et al. [4] also investigated the thermo-mechanical properties of CLT. They tested the fire performance of CLT walls and concluded the following:

- The most dominant failure mode in case of these walls was global instability with lateral deflections.
- The chosen adhesive and the number of plies were dominant factors in performance. The use of melamine urea formaldehyde was more advantageous compared to polyurethane. Five plies were proven better regarding fire performance compared to three plies with the same overall, due to the outer orthogonal layers (not contributing to load bearing) acted as “sacrificial layers”.
- CLT walls tend to lose their stability at artificial cooling phases similar to what Gernay [3] had documented for columns.

Hubbard and Salem [5] did experiments on the structural behaviour of a suggested new fully concealed moment resisting glulam connection utilizing mechanically fastened steel rods in different configurations under standard CAN/ULC-S101 [10] fire load. Their goal was to overcome a hindrance to wider utilization of timber in tall building construction. They measured different rod anchorage lengths and square shaped washer sizes. All four configurations reached 45 min fire resistance rating and one with the smaller washers and longer rod anchorage length reached the 60 min rating. Their research is a good example of the needed innovation for wider applicability of timber in taller buildings.

Tran et al. [6] examined spruce samples in a cone calorimeter and used the results for the creation and verification of a three step pyrolysis FE model. They used two different heat flux values (20 and 75 kW m⁻²) applied to compressed and uncompressed timber samples. They have concluded that the denser compressed wood had increased thermal conductivity, increased heat release rate and thermal inertia, while it had decreased the mass loss rate and charring rate compared to uncompressed samples. Their goal is to develop a predictive FE model for reducing the need for expensive experiments in case of dowelled joints.

Palma and Frangi [7] also examined dowelled timber joints in different configurations experimentally and also numerically. They highlighted the importance of both procedures because the number of parameters affecting each

other can make a seemingly simple problem quite difficult to solve with a purely analytical approach.

Charring rate of timber

Input parameters are crucial to all types of numerical analysis and charring rate is a particularly important factor in fire safety design of timber structures because it is the uncharred wood that carries the applied load in fire. Normally, it is calculated by dividing the charred distance by exposure time (Eq. 1).

$$\beta = \frac{d_{\text{char}}}{t} \quad (1)$$

where β is the charring rate, d_{char} is the charred depth, t is the exposure time.

Factors that influence the charring rate are the following [11]:

- Density
- Moisture content
- Specimens
- Permeability
- Oxygen concentration
- Grain direction
- Sample orientation
- Sample size
- Heat flux

Research results show that the mass loss rate has a spike after ignition and then decreases slowly as the exposure time increases (Fig. 1) [12]. This decrease happens due to the charred wood acting as thermal insulation. The process is not homogenous on a given surface because cracks appear in the charred volume where the heat and material transport are a lot faster.

Martinka et al. [13] concluded that mass loss and char depth have a linear relation in case of a constant heat flux.

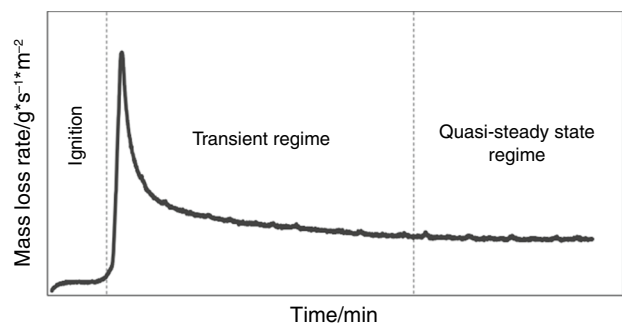


Fig. 1 Generic mass loss rate curve of timber at a steady heat flux from cone calorimeter testing [12]

The exact ratio of these two values depends on the density and therefore the species of the sample (Fig. 2). However, under constant heat flux, the time to char depth data is following a power regression curve, which is heat flux dependent [14] (Fig. 3).

Most national codes specify a constant charring rate for wood members in fire safety design. In North America, the generally used value in structural design without measurements for the specific material is $0.635 \text{ mm} \cdot \text{min}^{-1}$ for solid wood and glued-laminated timber (glulam) [15]. Eurocode 5 [8] gives a charring rate of $0.65 \text{ mm} \cdot \text{min}^{-1}$ for softwoods.

Charring rate is generally measured with a cone calorimeter or with bigger scale experiments with furnaces. The problem with these test methods is that they are relatively expensive and require specialized equipment.

However, there is a standard procedure to evaluate the durability of fire-retardant treatments. This procedure is the so-called Lindner test [16], which evaluates the efficiency by the mass loss due to the exposure of a small area of the sample surface to the combustion of 1 g of hexamethylenetetramine. This can be done on small cut-out samples from existing structures or samples taken from elements before installation. The test itself is cheap and does not require complex or heavy equipment. The method is not precise enough in itself to define charring rate for structural design in fire, but it might be with additional analysis of the geometry of the burnt part by computed tomography (CT). With such scans the geometry could be observed in 3D and with high precision (depending on the equipment).

CT for timber

It was already proven in the last few decades that CT is a great tool for human diagnostics, and it is gaining popularity in non-destructive material testing as well. Timber was first scanned in the early 1980s [17, 18] and the procedure and its use-cases have been in development ever since.

The species-based tomogram was first defined by Schwartz-Spornberger [19] and Wiebe [20] in the early

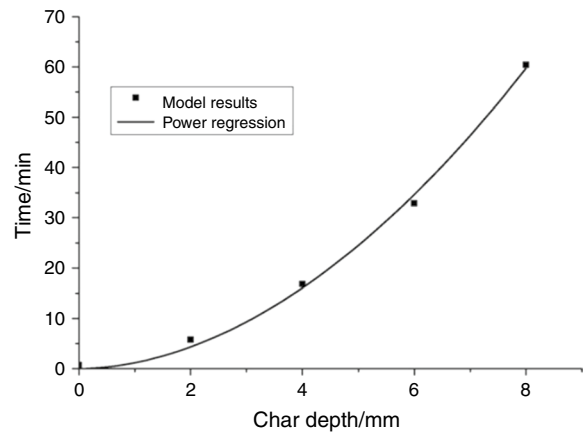


Fig. 3 Power regression of time and char depth under 40 kWm^{-2} constant heat flux [14]

1990s after several measurements with different species and Habermehl and Ridder [21, 22] described CT as a viable non-destructive imaging method to analyse whole tree cross sections. The species-based CT basically means that the density of the species varies greatly; therefore, the required image processing methods also differ in some cases.

The consideration to use CT in a sawmill environment also dates back to 1992, when Davis and Wells [23] discussed the methodology and the limitations of the measurement. Medical equipment in 1992 was already fast enough to test with and recreate the image from the data, but there was a limiting factor to them which was the spatial resolution of about 1 mm. At the time, they expected the development of the technology to be able to scan logs up to one meter in diameter. Mentioned limitations were the following:

- (1) Calibration difficulties as multiple scattering and beam hardening may be a problem,
- (2) Spatial resolution,

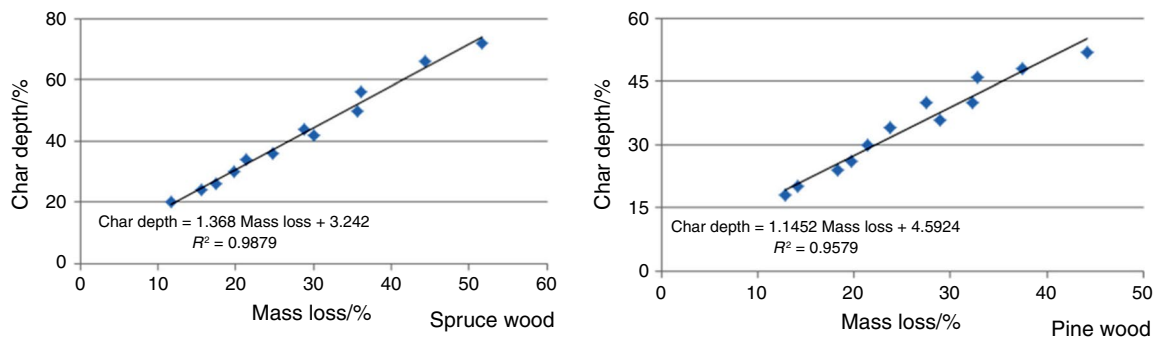


Fig. 2 Relationship between char depth and mass loss of spruce and pine timber [13]

- (3) Accuracy of the measurements because good resolution is not useful if the attenuation coefficients are not precise enough,
- (4) This measurement only provides linear attenuation coefficients therefore the understanding of involved physical processes, proper calibration and correlations methods are required to get more information about the specimens (e.g. water content or density).

The aforementioned limitation regarding spatial resolution is no longer an issue as the technology developed greatly. A voxel size of $1 \mu\text{m}^3$ can be achieved now if necessary for microstructural analysis [24].

Nowadays CT is used in the industry to measure water content, analyse the ring structure or find faults, which is useful to optimize the cuts in the sawmill. Automatic knot segmentation is essential for the use of CT in a sawmill environment, and there were many attempts to make it more precise and automated. Simple thresholding provides limited precision and value to the data; therefore, several markers and parameters are needed to be measured in the images (starting point, end point, length, inclination, azimuth, maximum diameter, volume) to better describe the location and also the other characteristics (size and inclination) of the knots [25]. The presence of wet sapwood also makes it more difficult to segment knots in a log, that is why the heavy use of morphology-based post-processing algorithms is necessary for accuracy in these cases [26].

Automatization is key when information for decision-making must be produced efficiently. A good example of this is the research of Philippe et al. [27], where they did a fast density measurement of wood density on increment cores by CT scanning. These measurements can help with the conversion of standing forests from volume to mass. This is useful for the evaluation of the forest regarding biomass, carbon stock and quality.

As mentioned in Longuetaud et al. [25] there was a demand for automatic species identification. The process is time consuming and is generally done by visual inspection and microscopy based in differences in anatomical features. With development of the technology and post-processing methods, high-resolution micro-CT became a viable alternative, in species identification as it can quickly produce the needed transverse, radial and tangential sections for analysis [28].

Goals

The main goal of this research was to verify the usability of a combination of two measurements (Lindner test and CT scan) to define charring rate. For this the charred volume had to be segmented. For verification, the volumes were compared to the mass loss during the Lindner test (described

in “[Lindner test](#)” Section). If the two measurements correlate, then in follow-up research, with the amount of heat the specimen was exposed to (known value) and with the mathematical description of the charred volume, the charring rate can be described on a plane with constant surface heat distribution. This method could be an alternative to measuring charring rate with big scale experiments in furnaces, and cone calorimeter tests. The test apparatus for the Lindner test is cheap and portable and medical grade CT equipment is widely available around the world. In this research, industrial CT (higher resolution) was used thus the applicability of medical grade equipment must be analysed in the future.

Methodology

For this research three different species were used (five specimens of each): spruce (*Picea abies*), ash (*Fraxinus excelsior*) and oak (*Quercus robur*). With the chosen species, there were two deciduous and one evergreen wood type available, all three having a different density. 100 mm long plate specimens were prepared with varying width and thickness, depending on the specific available product:

- Spruce— $100 \times 90 \times 10$ mm
- Ash— $100 \times 120 \times 19.9$ mm
- Oak— $100 \times 100 \times 22.7$ mm

The thickness can influence the charring by changing the heat capacity of the specimen which must be examined in the future, but the goal was to verify the usability of a method for different types of timber, not to compare charring rates of different species.

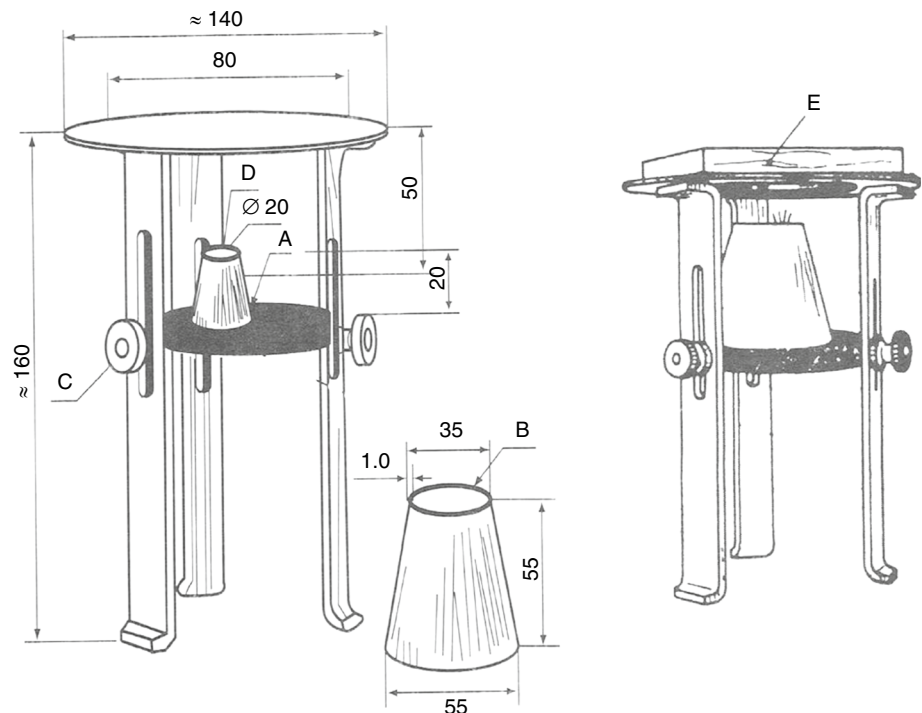
After the Lindner tests, the specimens were measured on a scale (to get mass loss data) and then they were CT scanned. The image sets were analysed by a MATLAB script (the image processing methods are described in “[Applied image processing methods](#)” Section). The goal was to segment the charred volumes and compare them to the measured mass loss data.

Lindner test

The Lindner test procedure is defined in the MSZ 9607 standard [16]. This method is used on-site to evaluate the effectiveness of fire-retardant materials on wood and wood-based products based on the mass loss due to charring. The test equipment is shown in Fig. 4.

For the test, 1 g of hexamethylene-tetramine ($\text{C}_6\text{H}_{12}\text{N}_4$) is placed on top of a small steel cylinder, then it is ignited. Right after the ignition, a half cone is placed over the cylinder to concentrate the heat transfer and this burns the timber specimen located on top of the equipment, above circle

Fig. 4 Lindner test equipment (A—steel burning block, B—chimney, C—adjusting screw, D—pastille, E—specimen) [16]



shaped hole 80 mm in diameter. The standard test specimen is $1 \times 10 \times 10$ cm. The amount of heat the timber is exposed to is set.

The evaluation happens based on mass loss due to the burning of the timber. The burning is not homogenous along the surface of the specimen, so the charring rate can only be given approximately.

CT scanning

X-ray computed tomography (CT) is a diagnostic method in radiology, which results in a spatial image. High-resolution non-destructive analysis can be problematic, optical or SEM methods only provide information about the surface of specimens.

CT uses X-rays and matching detectors to create the images, where the pixels are intensity values based on X-ray absorption of small volumes. The principle is that by scanning from multiple angles, these absorption profiles provide data to recreate the cross section. To make this possible, the ray source and the detector are rotated around the scanned object.

For the tests included in this paper, a custom-built industrial CT was used, which can use two different radiation sources and detectors depending on the use case (high resolution is needed or bigger objects are scanned) [29]. Timber scans were done using the macrofocus option with the following main parameters:

- Maximum object size: $800 \times 800 \times 1200$ mm

- Maximum thickness for aluminium: 160 mm
- Maximum thickness for steel: 80 mm
- Maximum thickness for polymers: 240 mm
- Resolution: $20 \mu\text{m} <$

Applied image processing methods

Digital image processing is a crucial step to analyse the CT image sequences and get useful information out of them. These algorithms are used to differentiate between various parts of the analysed material and the background (segmentation), reduce noise, define the analysed area (create a binary mask). There are a vast number of methods available and currently in development, because they are required for nowadays trivial, computer automated tasks like any kind of shape detection on images or even live video. A short summary of the used methods is given in the following.

To analyse a certain object in an image, a binary mask must be created first. This mask is the definition of which regions of an image later algorithms analyse or modify. This can be created in multiple ways. There are limiting methods (thresholding [30]) where the image is segmented into different zones based on a pixel intensity value or multiple intensity ranges (multilevel thresholding). With the proper density ranges these methods can help differentiate between certain objects or separate the foreground and the background of an image. With the combination of noise reduction methods discussed later, these limiting methods can be enough to identify the wanted object in an image, but in this current case it was not enough as the blocks between the

specimens (placed there because the specimens were stacked on top of each other and had to be spaced out for easier post-processing) were unfortunately too close in radiodensity to the timber samples. Thus, semi-manual region of interest (ROI) definition was used for all specimens (Fig. 5). The edges were defined manually at two opposite surfaces and the volume was created by an interpolation for each layer between them.

The next step was to differentiate between the charred part and the intact part of each specimen. Thresholding was used for this task. For the best result, the limits were set on a case-by-case basis, as some layers in the annual ring structure of the material were too close to the charred part in radiodensity. An example can be seen in Fig. 6, where a slight increase in the threshold limit value got rid of the lower density parts of the unburnt wood, while lower limit values still included charred wood. In such cases the disappearance of a little unburnt wood from the picture was favourable as it could be restored later.

The next step is noise reduction which was done using morphological closing (dilation followed by an erosion) and opening (erosion followed by a dilation). The closing of the image creates a closed down volume (closed boundary) using a predefined structuring element (strel object) [31]. This helps to recreate the parts of the unburnt wood with a follow-up filling operation. The morphological opening of the image uses a similar strel object but this gets rid of pixels or small pixel groups of the analysed binary mask which are too far from other pixels, so it gets rid of noise in the image [32].

The binary mask of the intact part was created with the functions described above. The next step was to create its complementary mask for the charred volume by subtracting

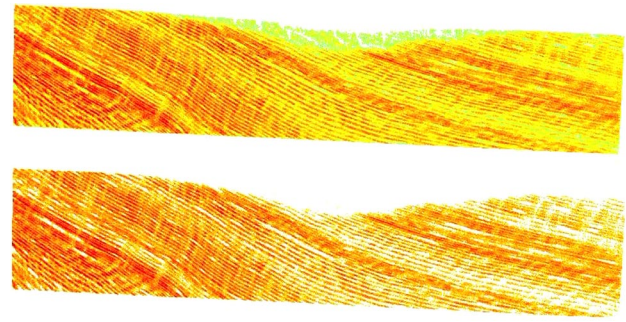


Fig. 6 Difference between $0.4 * \text{maximum pixel intensity}$ (top) and $0.5 * \text{maximum pixel intensity}$ (bottom) as threshold limit in case of an ash specimen, where the burnt segment is very close in radiodensity to the low density sections of the unburnt wood (colourized pictures for better visibility)

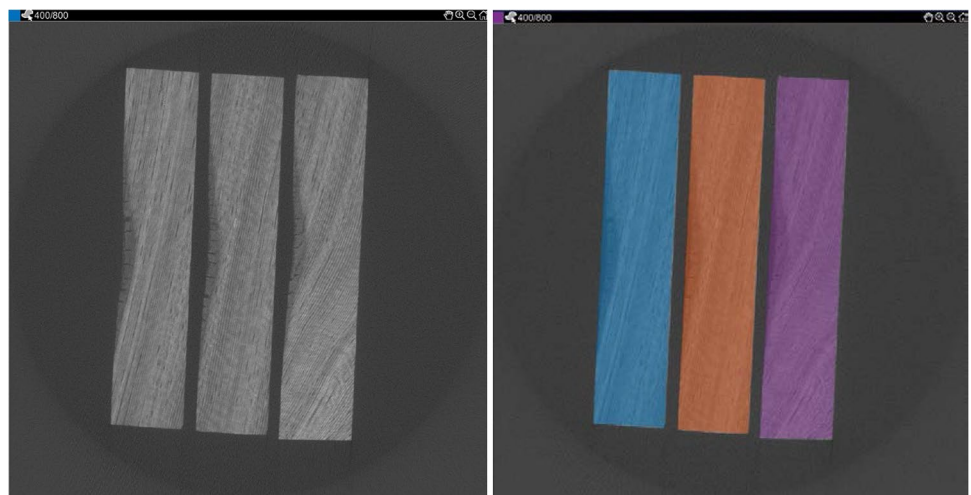
the intact part mask from the ROI for the whole specimen. Because of previous processes, there is a thin layer on the outer surface which should belong to the intact part, but it is associated with the charred volume. This must always be deleted from the charred part by a morphological opening and the known pixels be added to the intact part.

The results of the described digital image processing steps can be followed in Fig. 7.

Results

After visual observation it can be clearly seen that the charring is uneven on the surface as is expected from the test method and cracks appeared in the char (Fig. 8). The density and mass loss results are given in Table 1.

Fig. 5 Semi-manual region of interest (ROI) definition (raw image on the left, ROI masks on the right)



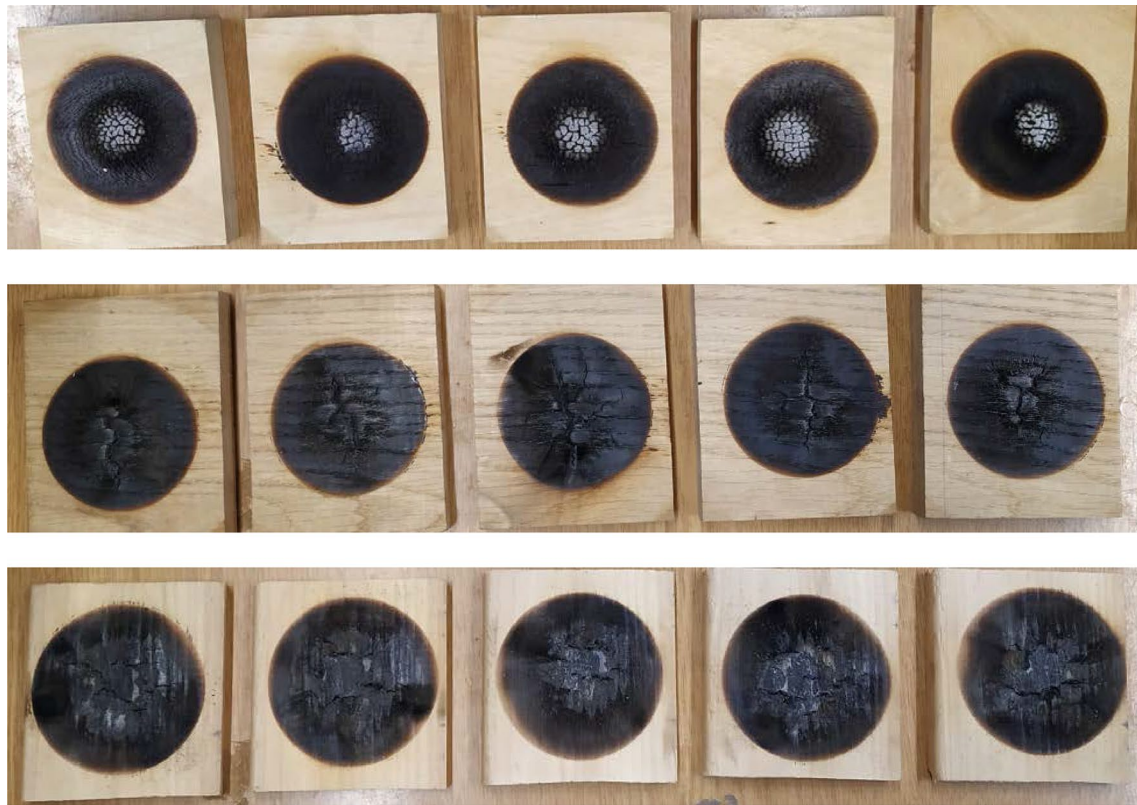


Fig. 7 Digital image processing steps to get binary masks for the intact and the burnt volumes

Results from the CT image sets are shown in Table 2. Ash samples got the ID “A”, oak samples the ID “O” and spruce samples the ID “S” for easier understanding. The results are also shown in Figs. 9, 10, 11 and 12. Spruce samples had the lowest density values paired with the highest relative mass loss and charred volume, but also had the lowest deviation (Table 3) in the measured results. This is notable given that there were two spruce samples with knots in the burned region, which were included to analyse the segmentation options in case of faults. The samples with the knots (S1 and S5 shown in Fig. 13) match the other spruce specimens in terms of the given metrics (low standard deviation as shown in Table 3). Considering these, the burnt volume segmentation itself was successful with the described methodology, the burnt part could be clearly separated.

Spruce specimens had the lowest density and radiodensity values (Figs. 11 and 12) and it is important to note that the deviation was also the lowest. In case of the S3

specimen, the mass loss and the burnt volume were lower than for the other spruce samples (Fig. 9.) Because of this, the burnt volumes are given relative to the mass loss values for better comparison (Fig. 10). In this figure, it becomes clear that even though the mass loss was lower in case of S3, the CT results follow as burnt volume/mass loss ratio is close to other spruce sample results. If the fraction of these two values has a low deviation among a group of similar samples, then the segmentation can be considered successful, but the difference between the two requires further analysis as for example water content can increase mass loss (the also heated but not yet burnt parts loose water), but that cannot be traced with image segmentation.

In case of the ash specimens the density values do not align with the radiodensity values (Figs. 11 and 12), A4 and A5 have noticeably lower radiodensity than the other 3, but this is not true for their measured density. This may be related to the significantly higher burnt volume

Fig. 8 Specimens after the Lindner test (from top to bottom: ash, oak and spruce) with cracks in the char

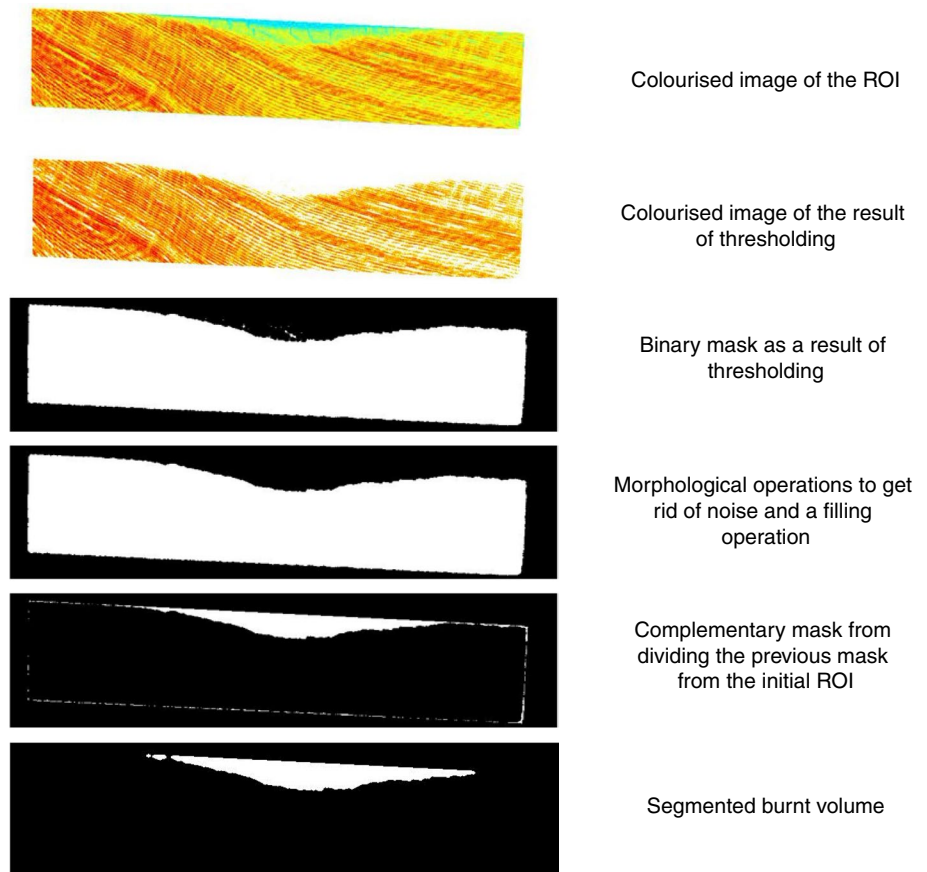


Table 1 Density before test and mass loss after Lindner test (A—ash, O—oak, S—spruce)

Specimen	Initial mass	Mass after Lindner test	Density	Mass loss	Relative mass loss/%
	/g	/g	/g * cm ⁻³	/g	
A1	144.43	140.26	0.601	4.17	2.89
A2	131.82	127.82	0.565	4	3.03
A3	134.51	130.37	0.575	4.14	3.08
A4	136.37	132.12	0.580	4.25	3.12
A5	134	129.3	0.571	4.7	3.51
O1	164.23	160.68	0.727	3.55	2.16
O2	160.05	156.1	0.721	3.95	2.47
O3	165.72	161.67	0.738	4.05	2.44
O4	176.85	172.79	0.784	4.06	2.30
O5	161.43	157.54	0.712	3.89	2.41
S1	36.31	33.37	0.393	2.94	8.10
S2	34.93	32.07	0.386	2.86	8.19
S3	35.72	33.29	0.387	2.43	6.80
S4	34.8	31.97	0.382	2.83	8.13
S5	35.11	32.31	0.380	2.8	7.97

for these two and the higher burnt volume relative to the mass loss (Table 2). It also must be noted that the ash and oak samples were not as homogenous as the spruce samples. There are regions where the annual ring structure is tighter resulting in local higher density, which have an effect on charring and CT analysis as well. The evaluation of these factors requires further analysis.

The oak specimens had a low deviation in mass loss, density and mean radiodensity as well (Table 3). In addition, the density and mean radiodensity values do align in this case, but the analysis of the CT scans regarding burnt volume draws a different picture. The deviation is the highest among the 3 tested species with a peak in the case of the O3 specimen (Fig. 9). While the deviation of the other four specimen's results is probably related to the inhomogeneous annual ring structure (similarly to the ash samples) of the oak, the third sample requires further study and possible refinement of the segmentation

Table 2 Results from CT image sets (A—ash, O—oak, S—spruce)

Specimen	Total volume / voxel count	Intact volume/ voxel count	Intact, mean radiodensity	Burnt volume./ voxel count	Burnt volume/%	Burnt mass loss/%	Burnt volume to mass loss/%
A1	92,391,235	90,684,961	31,077.54238	1,706,274	1.85	2.89	63.96
A2	91,932,938	90,103,133	30,951.49712	1,829,805	1.99	3.03	65.59
A3	93,313,649	91,213,179	32,286.92216	2,100,470	2.25	3.08	73.14
A4	92,954,969	90,716,368	27,303.8619	2,238,601	2.41	3.12	77.27
A5	90,739,839	88,194,872	27,357.55649	2,544,967	2.80	3.51	79.96
O1	96,243,909	95,125,661	33,102.34533	1,118,248	1.16	2.16	53.75
O2	94,437,493	93,363,979	32,910.10912	1,073,514	1.14	2.47	46.06
O3	95,252,810	93,233,125	32,347.06358	2,019,685	2.12	2.44	86.76
O4	94,158,334	92,879,101	34,585.16694	1,279,233	1.36	2.30	59.18
O5	95,049,895	93,608,484	33,032.38371	1,441,411	1.52	2.41	62.93
S1	45,547,072	43,203,506	19,889.59126	2,343,566	5.15	8.10	63.55
S2	45,240,114	42,880,012	19,768.80247	2,360,102	5.22	8.19	63.71
S3	46,648,047	44,844,020	19,656.1583	1,804,027	3.87	6.80	56.85
S4	44,035,592	41,858,918	19,736.10525	2,176,674	4.94	8.13	60.78
S5	47,223,923	44,849,590	19,437.62341	2,374,333	5.03	7.97	63.05

Fig. 9 Mass loss and burnt volume (A—ash, O—oak, S—spruce)

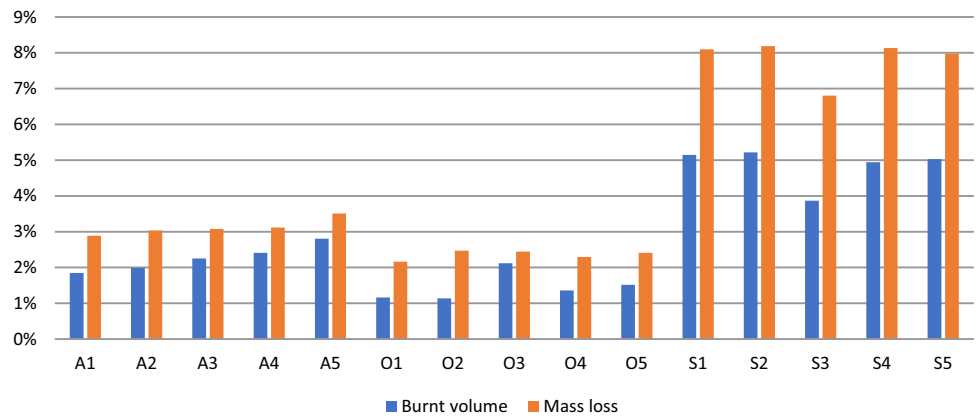
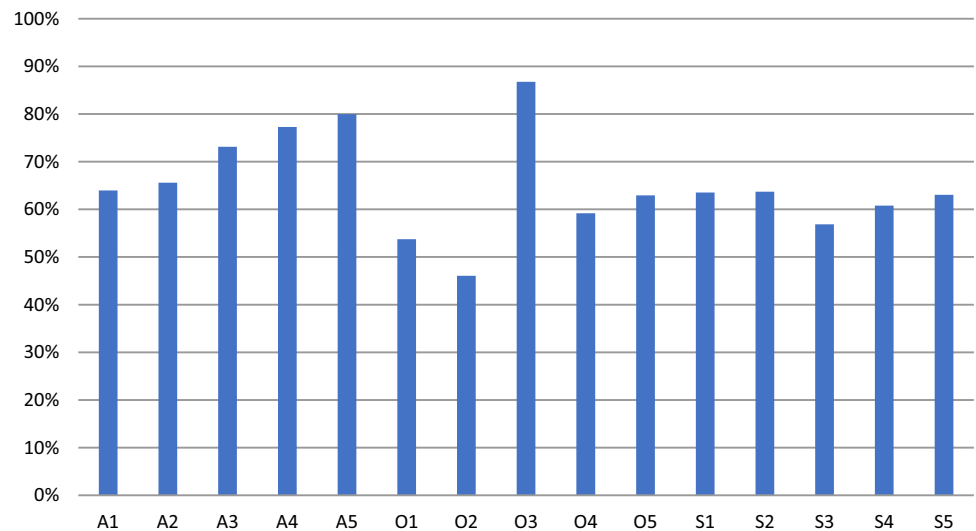


Fig. 10 CT measured volume loss relative to mass loss results (A—ash, O—oak, S—spruce)



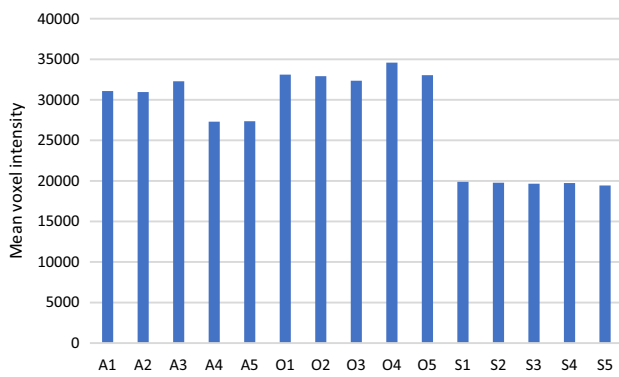


Fig. 11 Mean voxel intensity of the intact part, which is related to radiodensity and mean density of the samples (A—ash, O—oak, S—spruce)

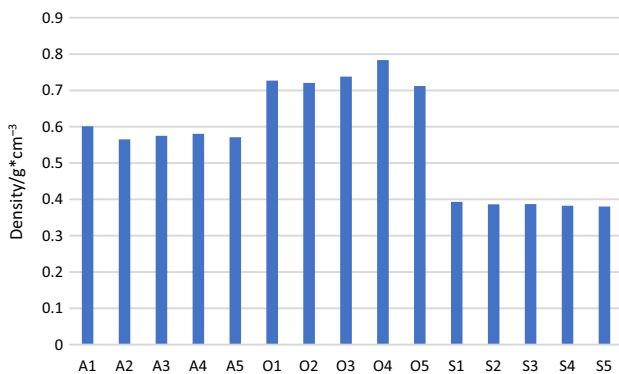


Fig. 12 Density of the samples (A—ash, O—oak, S—spruce)

Table 3 Mean values and standard deviation of the measurements by species for density, radiodensity, mass loss, burnt volume and the fraction of burnt volume to mass loss

Species	Density/g * cm ⁻³		Radiodensity		Mass loss		Burnt volume		Burnt volume/mass loss	
	Mean	St. dev	Mean	St. dev	Mean/%	St. dev/%	Mean/%	St. dev/%	Mean/%	St. dev/%
Ash	0.578	0.014	29,795	2310	3.12	0.23	2.26	0.37	71.99	7.04
Oak	0.736	0.028	33,195	832	2.36	0.13	1.46	0.40	61.74	15.36
Spruce	0.386	0.005	19,698	168	7.84	0.58	4.84	0.55	61.59	2.90

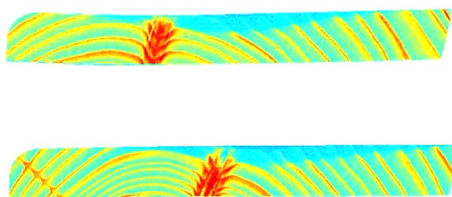


Fig. 13 Cross sections of S1 (top) and S5 (bottom) specimens, with the knots. CT scans were in correspondence with the mass loss results in case of these samples with knots in the burnt area

algorithm as well, even though coding errors and parameters were checked multiple times for this specific peak.

Conclusions

With the segmentation of the CT image sets, the burnt volumes could be separated properly in each case even when knots were present. Spruce samples provided the most consistent results regarding the mass loss/burnt volume. This is probably due to the uneven ring spacing and other inhomogeneities in the density of oak and ash. Although the samples were conditioned the same in the laboratory, water content might also be a factor when it comes to the standard deviation of the mass loss/burnt volume, but this requires further study.

The samples with the knots (S1 and S5) match the other spruce specimens in terms of the given metrics. Considering these, the burnt volume segmentation itself was successful with the described methodology, the burnt part could be clearly separated.

Results clearly indicate that a relatively simple test method such as the Lindner method can be used for the analysis of the charred layers of timber when combined with a 3D imaging technique such as X-ray computed tomography. An advantage of the measurement can be the relatively quick execution therefore enabling the analysis of bigger sample sizes.

For further development multilevel thresholding may be necessary to differentiate between different density regions in the intact part for later analysis. The use of medical grade

CT equipment must also be analysed later by scanning the same specimens on higher resolution industrial equipment and medical CT as well and comparing the results. It would provide a cheaper alternative to the CT scanning process. The effect of water content and local higher density regions must be evaluated by scanning the specimens before the Lindner test as well. If the aforementioned factors are dealt with, then a calibration of the results with cone calorimeter test is necessary and it can possibly be extended to samples with flame retardants, and wood-based products as well.

Acknowledgements The research reported in this paper is part of project no. BME-NVA-02, implemented with the support provided by the Ministry of Innovation and Technology of Hungary from the National Research, Development and Innovation Fund, financed under the TKP2021 funding scheme.

Author's contribution AB: Conceptualization, methodology, software, formal analysis, investigation, data curation, writing—original draft, visualization. ÉL: Resources, writing—review and editing, supervision.

Funding Open access funding provided by Budapest University of Technology and Economics.

Declarations

Conflict of interest The authors declare that they have no known competing financial interests or personal relationships that could have appeared to influence the work reported in this paper. The research reported in this paper is part of project no. BME-NVA-02, implemented with the support provided by the Ministry of Innovation and Technology of Hungary from the National Research, Development and Innovation Fund, financed under the TKP2021 funding scheme.

Open Access This article is licensed under a Creative Commons Attribution 4.0 International License, which permits use, sharing, adaptation, distribution and reproduction in any medium or format, as long as you give appropriate credit to the original author(s) and the source, provide a link to the Creative Commons licence, and indicate if changes were made. The images or other third party material in this article are included in the article's Creative Commons licence, unless indicated otherwise in a credit line to the material. If material is not included in the article's Creative Commons licence and your intended use is not permitted by statutory regulation or exceeds the permitted use, you will need to obtain permission directly from the copyright holder. To view a copy of this licence, visit <http://creativecommons.org/licenses/by/4.0/>.

7. References

- Regueira R, Martínez-Martínez JE, Alonso-Martínez M, Álvarez Rabanal FP, Guaita M, del Coz Díaz JJ. Experimental and numerical analyses of rounded dovetail timber connections (RDC) under fire conditions. *Eng Struct*. 2021;228:2020. <https://doi.org/10.1016/j.engstruct.2020.111535>.
- Kleinhenz M, Just A, Frangi A. Experimental analysis of cross-laminated timber rib panels at normal temperature and in fire. *Eng Struct*. 2021;246:113091. <https://doi.org/10.1016/j.engstruct.2021.113091>.
- Gernay T. Fire resistance and burnout resistance of timber columns. *Fire Saf J*. 2020;2021(122):103350. <https://doi.org/10.1016/j.firesaf.2021.103350>.
- Wiesner F, Hadden R, Deeny S, Bisby L. Structural fire engineering considerations for cross-laminated timber walls. *Constr Build Mater*. 2021;2022(323):126605. <https://doi.org/10.1016/j.conbuildmat.2022.126605>.
- Hubbard C, Salem O. Fire resistance of a fully concealed, moment-resisting new timber connection utilizing mechanically-fastened steel rods. *Fire Saf J*. 2022;129:103546. <https://doi.org/10.1016/j.firesaf.2022.103546>.
- Tran TT, Thi VD, Oudjene M, et al. Fire structural performance of thermo-mechanically compressed spruce timber by means experiments and a three-step multi-reactions pyrolysis 3D-finite element modelling. *Constr Build Mater*. 2021;2022(320):126100. <https://doi.org/10.1016/j.conbuildmat.2021.126100>.
- Palma P, Frangi A. Modelling the fire resistance of steel-to-timber dowelled connections loaded perpendicularly to the grain. *Fire Saf J*. 2019;107:54–74. <https://doi.org/10.1016/j.firesaf.2017.12.001>.
- EN 1995-1-2. Eurocode 5: design of timber structures—Part 1–2: general—structural fire design. 2013.
- EN 1995-1-1. Eurocode 5: design of timber structures - Part 1–1: General - Common rules and rules for buildings. 2004.
- CAN/ULC-S101. Standard methods of fire endurance tests of building construction and materials. 2014.
- Bartlett AI, Hadden RM, Bisby LA, Law A. Analysis of cross-laminated timber charring rates upon exposure to nonstandard heating conditions. *Fire Mater* 2015—14th Int Conf Exhib Proc. 2015, pp. 667–681.
- Morrisset D, Hadden RM, Bartlett AI, Law A, Emberley R. Time dependent contribution of char oxidation and flame heat feedback on the mass loss rate of timber. *Fire Saf J*. 2021;120:103058. <https://doi.org/10.1016/j.firesaf.2020.103058>.
- Martinka J, Rantuch P, Liner M. Calculation of charring rate and char depth of spruce and pine wood from mass loss. *J Therm Anal Calorim*. 2018;132(2):1105–13. <https://doi.org/10.1007/s10973-018-7039-8>.
- Lizhong Y, Yupeng Z, Yafei W, Zaifu G. Predicting charring rate of woods exposed to time-increasing and constant heat fluxes. *J Anal Appl Pyrolys*. 2008;81(1):1–6. <https://doi.org/10.1016/j.jaap.2007.06.006>.
- White RH. Charring rate of composite timber products. *Proc Wood Fire Saf*. 2000;353–364.
- MSZ 9607:2020. Égés-késleltető Szerrel Kezelt Fa És Fa Alapanyagú Építési Termékek Vizsgálata. A Kezelés Hatékonyságának Értékelése Lindner-Módszer Alapján.
- Gilboy WB, Foster J, Folkard M. A tomographic gamma-ray scanner for industrial applications. *Nucl Instrum Methods*. 1982;193:209–14.
- Kawamura H, Kogure J, Nakamura H, et al. Computed tomography for measuring annual rings of a live tree. *Proc IEEE*. 1983;71(7):907–8. <https://doi.org/10.1109/PROC.1983.12691>.
- Schwartz-Spornberger V. Untersuchungen an Bäumen Mit Hilfe Eines Computer—, Dissertation. Universität Marburg/Lahn. 1990.
- Wiebe S. Die Bedeutung der Holzfeuchte für die Wundbehandlung. In: Bad godesberger gehölzseminar, sachverständigenkuratorium, berichtsband. 1991.
- Habermehl A, Ridder HW. Computer tomographie am Baum Teil I: Erkennen der Baumfäule und Gerätekonzept. *Materialprüfung*. 1992;10:325–9.
- Habermehl A, Ridder HW. Computer tomographie am baum teil II: elektronische komponenten, systemsteuerung und anwendung. *Materialprüfung*. 1992;11–12:357–60.
- Davis J, Wells P. Computed tomography measurements on wood. *Ind Metrol*. 1992;2(3–4):195–218. [https://doi.org/10.1016/0921-5956\(92\)80004-D](https://doi.org/10.1016/0921-5956(92)80004-D).
- Van den Bulcke J, Masschaele B, Dierick M, Van AJ, Stevens M, Van HL. Three-dimensional imaging and analysis of infested coated wood with X-ray submicron CT. *Int Biodeterior Biodegrad*. 2008;61(3):278–86. <https://doi.org/10.1016/j.ibiod.2007.09.004>.
- Longuetaud F, Mothe F, Kerautret B, et al. Automatic knot detection and measurements from X-ray CT images of wood: a review and validation of an improved algorithm on softwood samples. *Comput Electron Agric*. 2012;85:77–89. <https://doi.org/10.1016/j.compag.2012.03.013>.
- Krähenbühl A, Kerautret B, Debled-Rennesson I, Mothe F, Longuetaud F. Knot segmentation in 3D CT images of wet wood. *Patt Recognit*. 2014;47(12):3852–69. <https://doi.org/10.1016/j.patcog.2014.05.015>.
- Jacquin P, Mothe F, Longuetaud F, Billard A, Kerfriden B, Leban JM. CarDen: a software for fast measurement of wood density

- on increment cores by CT scanning. *Comput Electron Agric.* 2019;156:606–17. <https://doi.org/10.1016/j.compag.2018.12.008>.
28. Kobayashi K, Hwang SW, Okochi T, Lee WH, Sugiyama J. Non-destructive method for wood identification using conventional X-ray computed tomography data. *J Cult Herit.* 2019;38:88–93. <https://doi.org/10.1016/j.culher.2019.02.001>.
29. Kozma I. Röntgen: CT Laboratórium; 2023. <https://att.sze.hu/rontgen-ct-laboratorium>. Accessed 23 Oct 2023
30. Gonzalez RC, Woods RE. *Digital image processing*. 4th edition; 2018.
31. Mathworks. Imclose—Morphologically close image. 2017. https://www.mathworks.com/help/images/ref/imclose.html?s_tid=mwa_osa_a. Accessed 5 Nov 2021.
32. Mathworks. Imopen: Morphologically open image. 2006. <https://www.mathworks.com/help/images/ref/imopen.html>. Accessed 5 Nov 2021.

Publisher's Note Springer Nature remains neutral with regard to jurisdictional claims in published maps and institutional affiliations.